Spectral and spatial characterization of a radio frequency power absorption in high pressure helicon plasmas

Konstantin P. Shamrai[a)]
Institute for Nuclear Research, National Academy of Sciences, 47 Prospect Nauki, Kiev 03680, Ukraine

Shunjiro Shinohara[b)]
Interdisciplinary Graduate School of Engineering Sciences, Kyushu University, Kasuga, Fukuoka 816-8580, Japan

(Received 2 March 2001; accepted 25 June 2001)

A power absorption in helicon plasma excited by double $m=0$ antenna is considered at high argon pressures, when the electron collision frequency exceeds the driving frequency. The influence of various factors is examined, including the plasma density and nonuniformity, magnetic field, gas pressure, and antenna spectrum. The wave dispersion curves and absorbed power spectra are comparatively examined to find out the scaling laws. The spatial distribution of the deposited power is characterized both qualitatively and quantitatively by considering the absorption profiles and fractions of the total power absorbed in the under antenna and edge regions of the plasma column. Dependencies of the plasma load resistance on various parameters and magnetic field profiles are examined and compared with experimental results. Computations are performed using two alternative models, either taking into account or neglecting the excitation of quasi-electrostatic Trivelpiece–Gould (TG) waves. Results on the plasma resistance are found to be close in both models provided collisional damping of helicons is not so low as to give rise to the cavity resonances. Inclusion of the TG waves yields magnetic field profiles which are substantially localized near the antenna, and absorption profiles strongly peaking in the peripheral plasma, underneath the antenna. With neglect of the TG waves, the magnetic fields and absorption profiles are found to be much more extended in both axial and radial directions from the antenna. Theory accounting for the TG waves gives a better fit over a broad range of parameters to the measured data, especially regarding the magnetic field profiles.
[DOI: 10.1063/1.1394779]

I. INTRODUCTION

The helicon discharge is extensively examined as an efficient source of dense low temperature plasmas for both basic research and numerous ground and space applications.[1,2] It is employed in materials processing (see, e.g., Refs. 3–5), and is expected to serve as an element for various tools, including a recent proposal of a plasma rocket for deep space missions.[6] The mechanisms of a radio frequency (rf) power absorption in helicon discharges are still under discussion in numerous papers. Since it became clear that direct collisional damping of helicons is much too weak to explain experiments,[7] two most frequently discussed mechanisms are the kinetic mechanism of electron acceleration by the helicon wave fields, and the fluid mechanism of the mode conversion of helicons into quasi-electrostatic waves. The electron acceleration has been examined both in a linear form, as the Landau damping of monochromatic wave[8] or as a transient wave-electron interaction in the antenna near field,[9] and in a nonlinear form as an electron trapping by the longitudinal electric field of the helicon wave.[10] The generation of accelerated electrons in helicon discharges has been confirmed in some experiments, but discarded in others (see discussion and references in Ref. 11).

The appearance of quasi-electrostatic waves, which are also referred to as the slow or Trivelpiece–Gould (TG) waves, is not self-evident in helicon plasmas. These waves are quasi-electrostatic and thus cannot be efficiently excited directly by the driving antenna via the mechanism of inductive coupling.[12] The group velocity resonance cone of TG waves, $\theta \approx \omega/\omega_{ce}$, where θ is an angle with respect to the magnetic field, ω the driving frequency, and ω_{ce} the electron gyrofrequency, is not a location of spatially resonant power flux from a line rf current source exciting a uniform, unbounded plasma.[13] However, the plasma boundary and/or the radial density gradient stimulate generation of the electrostatic activity. It arises as a response to the redundant plasma polarization produced by helicon electric fields and can be interpreted as the mode conversion of the helicon waves into TG waves. In uniform plasma, the surface conversion occurs at an abrupt interface of the plasma with insulating wall.[12] The absorption in this case is mainly provided by the TG waves and is maximum at the plasma boundary. The intensive generation of the TG waves underneath the antenna can give rise to the absorption hump, which extends along the group velocity resonance cone.[14,15] In nonuniform plasma,

a)Electronic mail: kshamrai@kinr.kiev.ua
b)Electronic mail: sinohara@aees.kyushu-u.ac.jp

the conversion occurs also in the bulk plasma, where it is enhanced in the regions of strong density gradient.[16,17] In this case, the source of the TG wave generation is not spatially localized, so that the contribution of the TG waves to the absorption profile is quite smooth and cannot be distinguished in computations from the contribution due to collisional damping of helicon waves.

The antenna coupling to and power absorption in helicon plasmas was theoretically examined using two different approaches based on the fluid plasma model. One of them is rigorous in that it includes the effect of electron inertia by employing the full dielectric tensor. Specific computations for radially uniform and nonuniform plasmas were performed using codes of two kinds: 1D codes which assume both axial and azimuthal plasma uniformity and use the Fourier decomposition of fields,[12,14,15,17–19] and 2D codes which include the axial nonuniformity and use the finite element method.[20,21] Obtained results clearly showed the generation of quasi-electrostatic activity in helicon plasmas. Another approach neglects the effect of electron inertia and thus automatically excludes the TG waves.[22,23] Both theoretical approaches were recently compared in detail for weakly collisional plasma.[24]

Although rigorous theory predicts generation of TG waves in helicon plasma, direct experimental evidence is not yet available. The reason is that these waves are normally very short scale in most experimental conditions. Another reason is that it is difficult to distinguish the contribution from the TG waves in standard measurements of the magnetic field profiles,[25] which is confirmed by computations.[24] A few experimental results reported so far provide an indirect evidence for the TG wave excitation in the range of low gas pressures where the ratio of electron collision-to-driving frequency is less than unity. These are recent measurements of the power balance in a conventional helicon discharge,[15] dispersion examination in a helicon discharge excited by flat antenna,[26] and comparative studies on the plasma load resistance.[11,27,28] Unfortunately, a detailed comparison of theory with experiment was not yet performed for the low pressure range.

A discharge at high pressures, where the electron collision frequency substantially exceeds the driving frequency and the electron mean free path is much shorter than the characteristic wavelength, has been examined less often although it is also of interest for applications.[29] A comparison of experimental results with theory based on the fluid model seems to be more credible in the high pressure range inasmuch as kinetic effects are suppressed. Systematic data on the behavior of helicon discharge at argon pressures up to 51 mTorr have been reported only recently,[30] and have been compared in detail with computations based on rigorous theory accounting for the excitation of the TG waves.[19] In those experiments, a long straight device immersed in a uniform magnetic field was used, so that a geometry of theoretical model was quite adequate for the experiment. Agreement of the results, including the antenna load resistance, magnetic field profiles, and thresholds for the density jumps, was shown to be pretty good over a broad range of operation parameters, in spite of the use of a uniform plasma model.[19]

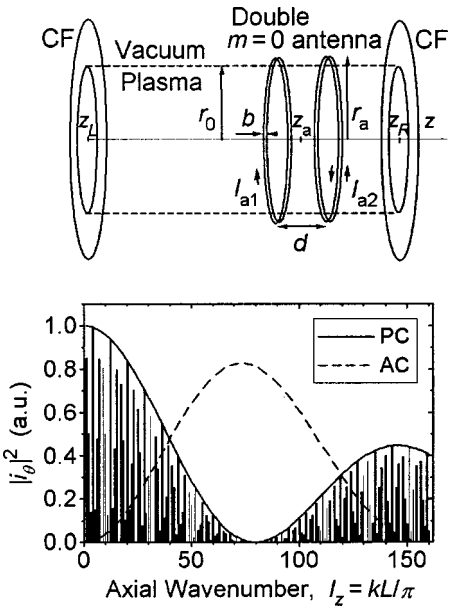

FIG. 1. A model of the helicon source excited by double-loop $m=0$ antenna (top), and normalized spectral intensity of the antenna current density (bottom). Column graph and solid curve are, respectively, the real spectrum and its envelope for the parallel currents (PC) in the antenna loops. Dashed curve is the spectral envelope for the anti-parallel antenna currents (AC). Conducting end-flanges are denoted as CF.

Another comparative study was recently performed with a similar device at argon pressure of 30 mTorr.[23] In general, satisfactory agreement was reported of the experimental data versus the load resistance, with results computed with use of theoretical approach neglecting the electrostatic waves.[22] In the present paper, we theoretically examine both approaches to ascertain the difference between them in the range of high pressures, and estimate the range of their validity by comparing the computed results with experimental data on the load resistance and magnetic field profiles.

The paper is organized as follows. Two theoretical models, both regarding and neglecting the TG waves, are introduced in Sec. II. Comparative analysis of the wave dispersion and power absorption spectra is presented in Sec. III. Profiles and quantitative characteristics of the spatial distribution of the rf power absorption are discussed in Sec. IV. Section V presents computed dependences of the plasma load resistance on various parameters. Experimental and theoretical results are compared in Sec. VI. In Sec. VII, we summarize the results and conclude.

II. THEORETICAL MODEL

To examine rf power absorption in $m=0$ helicon plasma, we use a theoretical model[31] generalized to include the effect of radial plasma nonuniformity. The plasma is considered as an axially uniform cylindrical column of length $L=z_R-z_L$, with two conducting flanges located at $z=z_R$ and z_L (see Fig. 1). The plasma is immersed in axial uniform magnetic field of strength B_0, and is confined radially by a thin nonconducting vessel of radius r_0. The radial plasma profile is assumed to be of parabolic form

$$n(r)=n_0-(n_0-n_{\mathrm{edge}})(r/r_0)^2, \tag{1}$$

where n_0 is the center density, and the edge density, $n_{\rm edge}$, can vary from 0 to n_0.

The double-loop $m=0$ antenna is centered at $z=z_a$ and consists of two identical radially thin rings, each of radius r_a and of finite width b, spaced a distance d apart. The rings contain rf currents equal in amplitude with parallel or anti-parallel directions, $I(t)=I_a\cos\omega t$. The ac fields in plasma and vacuum are described by Maxwell equations

$$c\nabla\times\mathbf{E}=-\partial\mathbf{B}/\partial t, \quad c\nabla\times\mathbf{B}=\partial\mathbf{D}/\partial t+4\pi\mathbf{j}_a, \tag{2}$$

where $\mathbf{j}_a=\hat{\boldsymbol{\theta}}i_a(z)\delta(r-r_a)\cos\omega t$ is the antenna current density, $\hat{\boldsymbol{\theta}}$ a unit vector in the azimuthal direction, and c the speed of light. As the plasma is supposed to be axially uniform, one can employ the Fourier decomposition over axial discrete wave numbers $k=l_z\pi/L(l_z=1,2,...)$[32,33]

$$i_a=\sum\ i_k\sin kz', \tag{3}$$

$$\mathbf{E}=2\,\mathrm{Re}\left\{\sum\ [\mathbf{E}_{\perp k}(r)\sin kz'+\hat{\mathbf{z}}E_{zk}(r)\cos kz'] \times\exp(-i\omega t)\right\}, \tag{4}$$

where $z'=z-z_L$, and $\hat{\mathbf{z}}$ is a unit vector in the axial direction. Series for the magnetic field $\mathbf{B}$ is similar to Eq. (4) but with $\sin kz'$ and $\cos kz'$ interchanged. Although each of harmonics in Eq. (4) represents an axial standing wave, the total field is not a standing wave inasmuch as the amplitudes are the complex functions in the presence of dissipation. Thus, the total field is found to be a combination of standing and traveling waves. Note that the form of series (4) implies vanishing of the tangential field on the conducting end-flanges. In the presence of sheath, the effective boundary condition can change.[34] However, this effect is inessential at high pressures because the waves radiated by the antenna are damped before reaching the ends. Computation results were found to be insensitive to the value of L.[19]

According to the results of measurements,[35] the distribution of the antenna current is well uniform across the rings. We assume also the azimuthal uniformity of current, that is, a charge-free or purely inductive coupling, $\nabla\cdot\mathbf{j}_a=0$. In the computations, the following geometric parameters were chosen to match the experiments[30]

$$z_a=-20\ \text{cm},\ d=2\ \text{cm},\ b=1\ \text{cm},\ r_0=2.5\ \text{cm},$$
$$r_a=3\ \text{cm},\ z_L=-80\ \text{cm}, \tag{5}$$

except that the length of the plasma column was assumed shorter than the experimental value, $L=160\,\text{cm}$ (i.e., $z_R=80\,\text{cm}$). This allows one to keep fewer harmonics and thus to save computation time without loss of accuracy. Indeed, at the high pressures under consideration the results do not suffer from parasitic reflections. With the above parameters, the antenna spectral intensity, $|i_k|^2$, is shown in Fig. 1 for the parallel and anti-parallel currents in the antenna loops. With parallel currents, a broad spectral minimum appears at $l_z\approx80$ due to the geometry of the antenna, which cannot excite harmonics with axial half-wavelengths around the distance between the antenna rings. A considerable decrease of the spectral intensity for $l_z>40$ is important for antenna coupling in some cases; it will be referred to as the ''depletion'' of the antenna spectrum. The spectrum is found to have a broken form with many local minima arising due to specific position of the antenna rings relative to the conducting ends. However, such spikes are not physically important: all the spatial distributions are found to be smooth provided that a sufficient number of harmonics is taken into account (see also Ref. 19). It is convenient to characterize the antenna spectrum by its envelope. In Fig. 1 are plotted the envelopes for both the parallel and anti-parallel current spectra.

Substituting series (4) into Maxwell equations (2) and introducing the dimensionless field amplitudes $\mathbf{e}_k$ and $\mathbf{b}_k$

$$\mathbf{E}_k(r)=(2\pi/c)i_k\mathbf{e}_k(r), \quad \mathbf{B}_k(r)=(2\pi/c)i_k\mathbf{b}_k(r),$$

one arrives at the following set of the first-order differential equations in cylindrical coordinates:

$$\begin{aligned} &NK_1e_z'=-iNK_2e_\theta+i(N^2-K_1)b_\theta,\\ &iN(\rho e_\theta)'=-\rho b_z,\\ &NK_1b_z'=i(K_1^2-K_2^2-N^2K_1)e_\theta+iNK_2b_\theta,\\ &iN(\rho b_\theta)'=K_3\rho e_z, \end{aligned} \tag{6}$$

where $N=kc/\omega$ is a longitudinal refractive index, the prime denotes the derivative with respect to the dimensionless radius $\rho=kr$, and the subscript k in the amplitudes is omitted for the sake of simplicity. The radial field components are expressed in an algebraic way

$$e_r=i(Nb_\theta-K_2e_\theta)/K_1, \quad b_r=iNe_\theta. \tag{7}$$

The permittivity tensor is considered in the cold plasma approximation

$$\begin{aligned} &K_1=1-\sum\ (\omega_{p\alpha}^2\gamma_\alpha/\Delta_\alpha),\\ &K_2=\sum\ (\omega_{p\alpha}^2\omega_{c\alpha}/\omega\Delta_\alpha), \quad K_3=1-\sum\ (\omega_{p\alpha}^2/\omega^2\gamma_\alpha), \end{aligned} \tag{8}$$

where the sum is over all species ($\alpha=e,i$), $\omega_{p\alpha}$ and $\omega_{c\alpha}$ are the plasma and cyclotron frequencies of species, respectively, and

$$\Delta_\alpha=(\omega\gamma_\alpha)^2-\omega_{c\alpha}^2, \quad \gamma_\alpha=1+i(\nu_\alpha/\omega). \tag{9}$$

The electron collision frequency takes into account the electron-neutral and electron-ion collisions, $\nu_e=\nu_{en}+\nu_{ei}$. In the range of electron temperatures 3–8 eV, the following approximation was used for the electron-neutral collisions in argon, $\nu_{en}\approx1.3\times10^6p_{\rm Ar}T_e\,(\text{s}^{-1})$, where $p_{\rm Ar}$ is Ar pressure, in mTorr, and T_e the electron temperature, in eV. The electron-ion collision frequency, ν_{ei}, was estimated from the Spitzer formula. Landau damping was found to be negligible at the high collisionality under consideration.[19] In the computations, we put $\nu_i/\omega=0.1$ and employed the following parameters, which are close to the experimental values: driving frequency $\omega/2\pi=7$ MHz, electron temperature $T_e=4$ eV, and Ar pressure $p_{\rm Ar}=6$ and 51 mTorr.[30]

To find the fields, one should solve, for each of harmonics, Eqs. (6) in the plasma and similar equations (with K_1

$=K_3=1$ and $K_2=0$) in the gap between the plasma surface and the antenna, at $r_0<r<r_a$, and in the region outside the antenna, at $r>r_a$. (The outer boundary is assumed at infinity.) These solutions are joined by imposing the following conditions on the tangential fields: (i) continuity of all field components at $r=r_0$, and (ii) the continuity at $r=r_a$ of all components except for the b_z field, which has to satisfy the condition $b_z(r_a+0)-b_z(r_a-0)=-1$.

Solutions to Eqs. (6) in the radially uniform plasma are readily found as combinations of the Bessel functions $J_{0,1}(k_\perp r)$ where the perpendicular wave number $k_\perp$ acquires the two values, k_H and k_{TG}, which relate to the helicon and TG waves.[31] These values are the roots of an exact biquadratic (relative to both $k_\perp$ and k) dispersion equation.[36] With a nonuniform plasma profile, Eqs. (6) were numerically integrated using Mathematica 3.0. The computation scheme was similar to that reported in Ref. 17: nonsingular (at $r=0$) fundamental solutions were found with the initial conditions taken at $r=r_{\min}\ll r_0$ as appropriate values of the uniform solutions. Outside the plasma, analytical solutions were used as combinations of the modified Bessel functions. The total fields were computed by making the finite sums (4) over l_z ranging 1 to some maximum wave number, $l_{z\max}$. In each case, $l_{z\max}$ was optimized to avoid the instability of computation for very short modes, but to hold accuracy to a reasonable level of a few percent.

The rate of work done by the $m=0$ antenna current to excite the fields, $P=-\int j_a E_\theta\, dV$, where $E_\theta(r,z,t)$ is the azimuthal electric field and the integration is over volume, can be expressed as the product of the antenna current and antenna voltage, $I(t)U(t)$. Using Eqs. (3) and (4) and integrating yields the complex load impedance of the antenna defined as a proportionality coefficient between the complex amplitudes of the antenna voltage and current

$$Z_a=-\frac{4\pi^2 r_a L}{cI_a^2}\sum |i_k|^2 e_{\theta k}(r=r_a). \tag{10}$$

The real and imaginary parts of the impedance, $Z_a=R_a-iL_a$, represent the antenna load resistance and inductance, respectively.

The specific power absorbed in the plasma is

$$p_a=\frac{\omega}{2\pi}\mathrm{Im}[K_1|\mathbf{E}_\perp|^2+K_3|E_z|^2+2K_2\,\mathrm{Re}(E_r E_\theta^*)], \tag{11}$$

where the asterisk denotes the complex conjugate. The total power absorbed in the plasma, P_a, is the integral of p_a over the plasma volume. It may be written as $P_a=(1/2)R_p I_a^2$, where the plasma load resistance is the sum of partial resistances over l_z

$$R_p=\sum R(l_z). \tag{12}$$

As long as the emission of electromagnetic waves outside the system and losses in the antenna circuit and metal environment are neglected, the following equality holds $R_p=R_a$. Since R_p is the integral characteristic whereas R_a is defined by the boundary value of the azimuthal electric field, this equality can be used for checking on the accuracy of computations.[24] Computation errors of this sort were found to be well below 1%, in spite of the fact that the fields vary extremely steeply at high collisionality considered. The plasma load reactance is defined as $L_p=L_a-L_v$ where L_v is the vacuum (without plasma) load reactance.[27]

Along with the above rigorous model, we have also considered a simplified approach taking only the helicon waves into account. Following Ref. 24, we will refer to these models as to the helicon—Trivelpiece–Gould (H-TG) and transverse electric–helicon (TE-H) approximations, respectively. In the TE-H approach, it is assumed that $E_z=0$, so that the first Eq. (6) acquires an algebraic form whereas the last Eq. (6) is dropped from the set. Thus, the TE-H approach proceeds from solving of two equations instead of system (6)[22,24]

$$iN(\rho e_\theta)'=-\rho b_z, \quad b_z'=-iNQe_\theta, \tag{13}$$

where $Q=[(N^2-K_1)^2-K_2^2]/N^2(N^2-K_1)$. The rest of the field components are expressed as

$$e_r=iK_2 e_\theta/(N^2-K_1), \quad b_r=iNe_\theta, \quad b_\theta=-iNe_r. \tag{14}$$

The computation procedure and accuracy control were similar to those described above.

III. WAVE DISPERSION AND ABSORPTION SPECTRA

To interpret the spectra and profiles of rf power absorption, it is helpful to examine the wave dispersion in the uniform unbounded plasma approximation by using the dispersion relation in the form $k_\perp=F(k,B_0,n_0,\nu_e)$ where $k_\perp=k_r+ik_i$ is the complex perpendicular wave number, and the parallel wave number k is considered as a real variable. At zero collisions, this equation defines the regions of parameters in which the waves are propagating ($\mathrm{Im}\,k_\perp=0$) or evanescent ($\mathrm{Im}\,k_\perp\neq 0$). In the latter case, the fields exponentially decay from the source even at zero collisions, with a penetration depth k_i^{-1}.

At low magnetic fields, $\omega_{ce}\ll\omega|\gamma_e|$, the plasma is actually unmagnetized and thus isotropic. For an axially uniform mode with $k=0$, the following relation (see, e.g., Ref. 37) defines the penetration depth

$$\delta_c=(c/\omega)\mathrm{Im}(K_3)^{-1/2}\approx\delta\left\{2\,\frac{1+(\nu_e/\omega)^2}{1+[1+(\nu_e/\omega)^2]^{1/2}}\right\}^{1/2}, \tag{15}$$

where $\delta=c/\omega_{pe}$ is the collisionless skin depth at $B_0=0$. Equation (15) shows a transition from the collisionless to collisional skin effect: the penetration depth monotonically increases with ν_e. For the mode with finite axial wave number, the depth takes the form $(c/\omega)\mathrm{Im}(K_3-N^2)^{-1/2}$, where $N=kc/\omega$. It decreases with increasing k, as shown in Fig. 2(a). The power absorption spectrum; that is, the dependence of the partial resistance on axial wave number $R(l_z)$ [see Eq. (12)], is shown in Fig. 2(b) for the excitation with parallel antenna currents. As the spectrum keeps the same fine structure as the antenna spectrum (compare Fig. 1), it is suitable to consider the spectral envelope also shown in Fig. 2(b). The spectral intensity rapidly drops with increasing k and

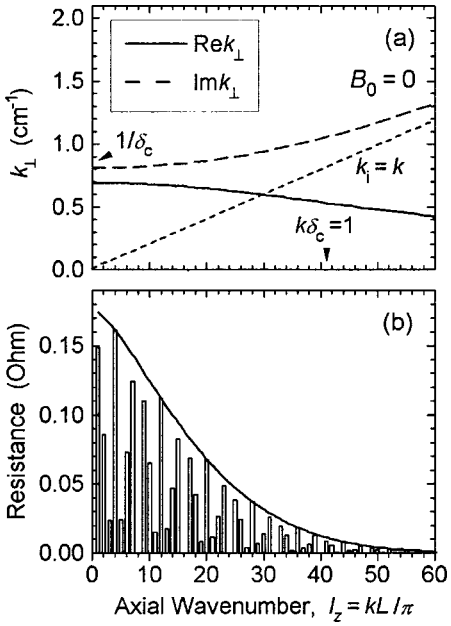

FIG. 2. Spectral characteristics for an unmagnetized uniform plasma. (a) Dispersion curves of oscillations and asymptote $k_i = k$. (b) The power absorption spectrum (column graph) and its envelope (solid curve), for the parallel currents in the antenna loops. $p_{\mathrm{Ar}} = 51$ mTorr and $n_0 = 2 \times 10^{12}$ cm^{-3}.

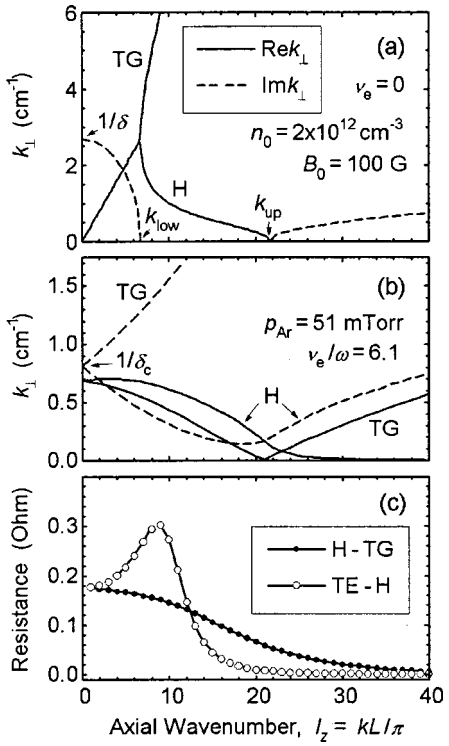

FIG. 3. Spectral characteristics for a magnetized uniform plasma. Wave dispersion curves at (a) zero collisions, and (b) Ar pressure of 51 mTorr. H and TG denote the helicon and TG dispersion branches, respectively. (c) Envelopes of the power absorption spectra computed with H-TG and TE-H models, at parallel antenna currents and $p_{\mathrm{Ar}} = 51$ mTorr, $B_0 = 100$ G and $n_0 = 2 \times 10^{12}$ cm^{-3}.

vanishes for $l_z > 40$, due to both the decrease of the penetration depth and the ''depletion'' of the antenna spectrum. Note that a finite gap between the antenna and plasma also reduces the contribution of the higher modes to the absorption.[19]

At higher magnetic fields, $\omega_{ce} \gg \omega |\gamma_e|$, the plasma is magnetized and thus anisotropic. In this case, $k_\perp$ can be evaluated from the solution to either the exact biquadratic equation[36] or to the following approximate quadratic equation:

$$[k_t k(\omega_{ce}/\omega) - k_t^2 \gamma_e]\delta^2 = 1, \tag{16}$$

where k_t is the total wave number. Equation (16) is valid provided $\omega_{LH} \ll \omega \ll \omega_{pe}$ where ω_{LH} is the lower hybrid frequency, and $\omega_{ce} \ll \omega_{pe}$, so that the components of the permittivity tensor Eq. (8) take an approximate form

$$K_1 \approx \omega_{pe}^2 \gamma_e / \omega_{ce}^2, \quad K_2 \approx -\omega_{pe}^2/\omega\omega_{ce}, \quad K_3 \approx -\omega_{pe}^2/\omega^2\gamma_e. \tag{17}$$

As long as Eq. (16) includes all the wave numbers multiplied by δ, this provides a scaling of the dispersion curves with density. Although this approximate scaling neglects the variation of ν_e with density through the Coulomb collisions, it is quite good at high pressures.

In the axially uniform case, $k = 0$, the penetration depths are known to differ for the electric field polarized along (TM polarization) and across (TE polarization) the static magnetic field (see, e.g., Ref. 37)

$$\delta_\parallel = \delta_c, \quad \delta_\perp = (c/\omega)\mathrm{Im}[(K_1^2 - K_2^2)/K_1]^{-1/2}. \tag{18}$$

However, for dense plasmas, when relations (17) are true, one arrives at $\delta_\perp \approx \delta_\parallel = \delta_c$, so that the effect of magnetic field is of no account for the penetration of axially uniform fields.

A finite axial wave number, even if it is quite small $k \gtrsim (\omega/\omega_{ce}\delta)$, substantially changes the dispersion. In this case, Eq. (16) describes the oscillations of two different kinds, that is helicon and Trivelpiece–Gould (TG) waves. At zero collisions, their dispersion curves are shown in Fig. 3(a). Propagating helicon waves are known to exist in a finite region of axial wave numbers[12]

$$k_{\mathrm{low}} < k < k_{\mathrm{up}}, \tag{19}$$

where

$$k_{\mathrm{low}} = \delta^{-1} 2(\omega/\omega_{ce}) \quad \text{and} \quad k_{\mathrm{up}} = \delta^{-1}(\omega/\omega_{ce})^{1/2}. \tag{20}$$

The upper boundary of this region is a cutoff for helicons ($k_\perp \to 0$ at $k \to k_{\mathrm{up}}$). Short helicons, $k > k_{\mathrm{up}}$, are purely evanescent oscillations, $k_r^{(H)} = 0$. The branch of propagating TG waves exists at $k > k_{\mathrm{low}}$, and merges to the helicon branch at $k = k_{\mathrm{low}}$. Both waves are evanescent in the long wave region, $k < k_{\mathrm{low}}$, where they have real wave numbers opposite in sign, $k_r^{(H)} = -k_r^{(\mathrm{TG})}$, and equal k_i which tends to $1/\delta$ at $k \to 0$. The modes in this region subject to a magnetic field reduced collisionless skin effect, that is have penetration depths exceeding δ.

Figure 3(b) shows the dispersion curves calculated at high collisionality, $p_{\mathrm{Ar}}=51$ mTorr. The TG waves decay at a short distance which is less than both δ_c and the wavelength[31]

$$k_i^{(\mathrm{TG})} \approx k \nu_e \omega_{ce} (\omega^2 + \nu_e^2)^{-1} \gg k_r^{(\mathrm{TG})}. \tag{21}$$

On the contrary, helicons are extremely weakly damped waves. Inside the propagation region Eq. (19) the following approximate relation is true:[12]

$$k_i^{(H)} \approx \nu_e k^{-3} \delta^{-4} \omega^2 \omega_{ce}^{-3} \propto \nu_e n_0^2 B_0^{-3}. \tag{22}$$

One can see from Fig. 3(b) that at 51 mTorr the helicons still exist as propagating waves ($k_i^{(H)} < k_r^{(H)}$) over all the region $k < k_{\mathrm{up}}$, except for its long wavelength part where they suffer from the reduced collisional skin effect. At $k \to 0$, the penetration depths for both waves become equal to that for an unmagnetized plasma, δ_c. The helicon branch of $\mathrm{Im}\, k_\perp$ has a minimum at $k \lesssim k_{\mathrm{up}}$. At $k > k_{\mathrm{up}}$, the graph of $k_i^{(H)}$ rapidly approaches to that for unmagnetized plasma, $k_i \approx k$. Very short helicon modes are similar to the evanescent vacuum TE modes, and are insensitive to both collisions and the magnetic field.

Figure 3(c) shows the envelope of the power absorption spectrum computed with the H-TG model (solid circles). As compared with the case of unmagnetized plasma, the spectral amplitudes are practically the same for the lower modes, $k < k_{\mathrm{low}}$, but are found to be enhanced for the intermediate modes, Eq. (19), whereas they are reduced for evanescent modes, $k > k_{\mathrm{up}}$. Thus, the spectrum is cut above k_{up} rather than above $1/\delta_c$, as it is at $B_0 = 0$. Inasmuch as $k_{\mathrm{up}} \delta_c \approx (\nu_e / \omega_{ce})^{1/2} < 1$, the magnetic field gives rise to narrowing of the k-spectrum. The envelope of the absorption spectrum computed with alternative, TE-H model is shown in Fig. 3(c) by open circles. In contrast with the H-TG spectrum, it drops more rapidly for the short modes and demonstrates the maximum at intermediate k. It arises from the first radial cavity resonance, as was found by considering an approximate dispersion relation for the helicon eigenmodes, $B_z(r = r_0) = 0$,[24] which yields the following condition for the pth radial resonance of the $m = 0$ mode:

$$k \approx k_{\mathrm{res}} = r_0 \omega \omega_{pe}^2 / q_p c^2 \omega_{ce}, \tag{23}$$

where the numerical factor q_p refers to the pth root of J_0 ($q_1 \approx 2.40$, $q_2 \approx 5.52$,...).

As long as the dispersion curves scale approximately with density as $\delta^{-1} \sim n_0^{1/2}$, one can deduce their behavior at higher (lower) density by extending (shrinking) the graphs in Fig. 3 along both axes. Figure 4(a) shows the dispersion curves computed for the same conditions as in Fig. 3(b) but at higher density $n_0 = 1 \times 10^{13}\,\mathrm{cm}^{-3}$. The graphs look similar to those in Fig. 3(b), since the limits along both axes were deliberately scaled up as $n_0^{1/2}$. The envelope of the H-TG absorption spectrum is shown in Fig. 4(b) (solid circles). As compared with Fig. 3(c), a steeper drop of the spectrum occurs for higher harmonics, due to the "depletion" of the antenna spectrum. The envelope of the TE-H absorption spectrum, which is shown in Fig. 4(b) by open circles, has a maximum arising from the first radial cavity resonance. A small hump corresponding to the second radial resonance is also seen at lower k.

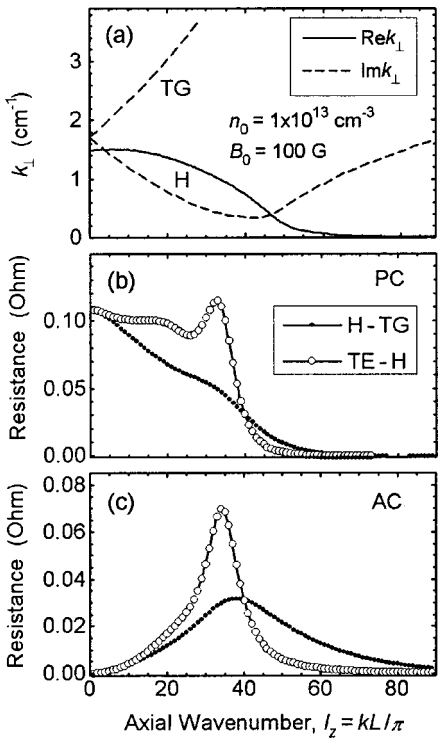

FIG. 4. Dispersion curves (a) and envelopes of the absorption spectra at parallel (b) and anti-parallel (c) antenna currents, for the uniform plasma. $p_{\mathrm{Ar}} = 51$ mTorr, $B_0 = 100$ G, and $n_0 = 1 \times 10^{13}\,\mathrm{cm}^{-3}$.

Figure 4(c) shows the envelopes of the absorption spectrum for anti-parallel antenna currents. The H-TG envelope has a maximum, which arises in a competition of the increasing intensity of the antenna spectrum and decreasing excitation capacity of the short modes. One can see that absorption spectrum is low at $k > k_{\mathrm{up}}$, in spite of that the antenna spectrum grows up to $l_z \approx 80$ (see Fig. 1). Thus, the effect of the wave dispersion strongly predominates over the effect of antenna spectrum. The maximum of the TE-H spectrum in Fig. 4(c) arises from the cavity resonance, at the same k as in the case of parallel excitation.

Figure 5 demonstrates changes of the dispersion and absorption spectrum with varying gas pressure (collision frequency) and magnetic field. Plots in Figs. 5(a) and 5(b) were computed for the same conditions as in Fig. 3, but at lower Ar pressure of 6 mTorr ($\nu_e / \omega \approx 0.9$). One can see from Fig. 5(a) that the effect of pressure differs substantially for the different parts of the helicon dispersion curve. As compared with the case of 51 mTorr (see Fig. 3), the penetration depth is lower for the long helicon modes, $k < k_{\mathrm{low}}$, as a result of decreased δ_c. On the contrary, the depth is substantially higher for the intermediate modes, $k_{\mathrm{low}} < k < k_{\mathrm{up}}$ in agreement with Eq. (22). The branch of evanescent helicon modes, $k > k_{\mathrm{up}}$, is practically insensitive to pressure. The penetration depths of the TG waves are much lower at 6 mTorr than at 51 mTorr [compare Figs. 3(b) and 5(a)]. Indeed, Eq. (21) says that damping of the TG modes peaks at $\nu_e / \omega \approx 1$, which is just the case at 6 mTorr. The envelope of the absorption

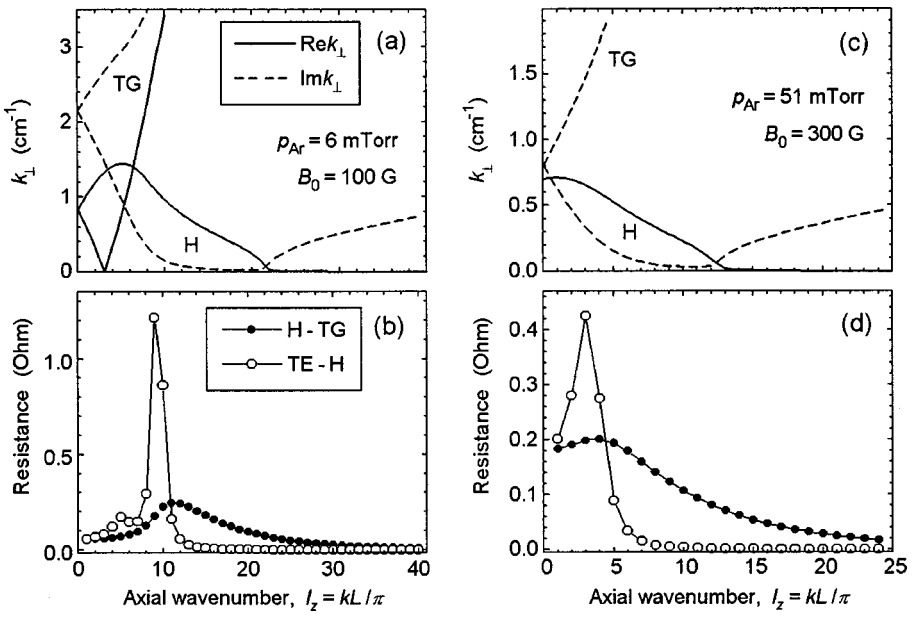

FIG. 5. Dispersion curves (top) and envelopes of the absorption spectra (bottom), for the uniform plasma of density $n_0 = 2\times10^{12}\,\mathrm{cm}^{-3}$, at parallel antenna currents. (a) and (b): $p_{\mathrm{Ar}}=6$ mTorr and $B_0=100$ G; (c) and (d): $p_{\mathrm{Ar}}=51$ mTorr and $B_0=300$ G.

spectrum computed with H-TG model is shown in Fig. 5(b) (solid circles). The absorption is suppressed for the lower harmonics from the region of reduced skin effect, $k<k_{\mathrm{low}}$, because damping of these modes is stronger than at 51 mTorr. The absorption clearly maximizes for the modes with k well below k_{up}, rather than for those modes which have the maximum penetration depths. This results from the fact that in the H-TG model a principal part of the input power is absorbed through the mode conversion of helicons into electrostatic TG waves.[12,17] In uniform plasma, the conversion occurs at a plasma boundary where the radial electron current must vanish. This yields the following relation between the amplitudes of the helicon and TG waves[16]

$$E_r^{(\mathrm{TG})} \approx i(\omega_{ce}/\gamma_e\omega)E_\theta^{(H)} \quad \text{at } r=r_0. \tag{24}$$

So, the amplitude of the TG wave and thus the absorption due to conversion is maximum provided $E_\theta^{(H)}$ is maximum at the boundary. As long as $E_\theta^{(H)}\sim J_1(r\omega\omega_{pe}^2/kc^2\omega_{ce})$, the maximum absorption occurs for the modes with axial wave numbers

$$k\approx k_{\max}=r_0\omega\omega_{pe}^2/1.84c^2\omega_{ce}, \tag{25}$$

where the numerical factor 1.84 corresponds to the first maximum of J_1. Equation (25) is found to predict well the maximum of the H-TG spectrum in Fig. 5(b). The absorption spectrum dramatically changes in the TE-H approximation [open circles in Fig. 5(b)]. As a result of low helicon damping, the spectrum has a sharp maximum relative to the first radial cavity resonance, and a small maximum, at lower k, corresponding to the second radial resonance. Positions of these resonances are in a good agreement with Eq. (23).

The effect of increasing magnetic field on the wave dispersion is seen from Figs. 5(c) and 5(d) computed at the same conditions as Fig. 3, but at $B_0=300$ G. The right boundary for the propagating helicons, k_{up}, shifts toward lower harmonics, and damping of intermediate helicon modes decreases, in agreement with Eqs. (20) and (22). The magnetic field weakly affects damping of evanescent helicons, $k>k_{\mathrm{up}}$. Damping of the TG modes is stronger at higher B_0, as seen from Eq. (21). The envelope of the H-TG absorption spectrum [solid circles in Fig. 5(d)] is found to be narrower than at 100 G and much narrower than at zero magnetic field. The TE-H absorption spectrum [open circles in Fig. 5(d)] maximizes at the first radial resonance.

The influence of the plasma nonuniformity on the absorption spectra is seen from Fig. 6 computed with parabolic density profile Eq. (1). With decreasing edge density, the spectra computed with both models decrease for the short modes whereas increase for the long modes. This is due to the decrease of mean density in the plasma column, which is followed by the decrease of the effective upper boundary for

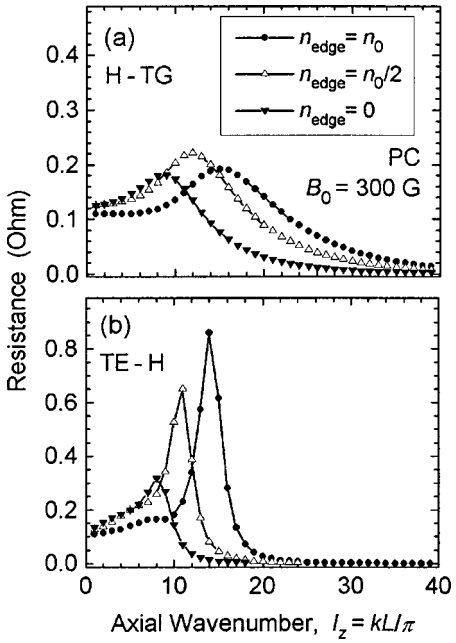

FIG. 6. Envelopes of the absorption spectra computed for a nonuniform plasma with (a) H-TG and (b) TE-H models, at parallel antenna currents. $p_{\mathrm{Ar}}=51$ mTorr, $B_0=300$ G, and $n_0=1\times10^{13}\,\mathrm{cm}^{-3}$.

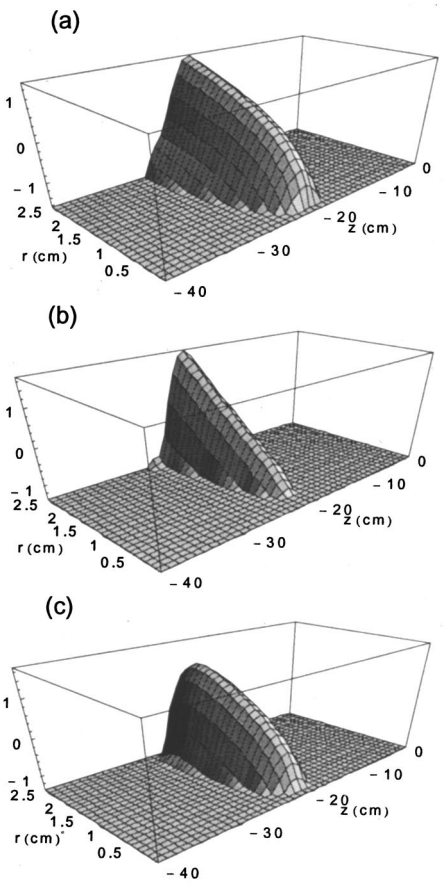

FIG. 7. Profiles of the absorbed power, $\log_{10}(p_a)$ with p_a in mW/cm^3, for an unmagnetized plasma excited with parallel antenna currents, at $p_{\mathrm{Ar}}=51$ mTorr. Uniform plasma of density (a) $n_0=2\times10^{12}\,\mathrm{cm}^{-3}$ and (b) $n_0=1\times10^{13}\,\mathrm{cm}^{-3}$; and (c) nonuniform plasma with center density $n_0=1\times10^{13}\,\mathrm{cm}^{-3}$ and edge density $n_{\mathrm{edge}}=0$.

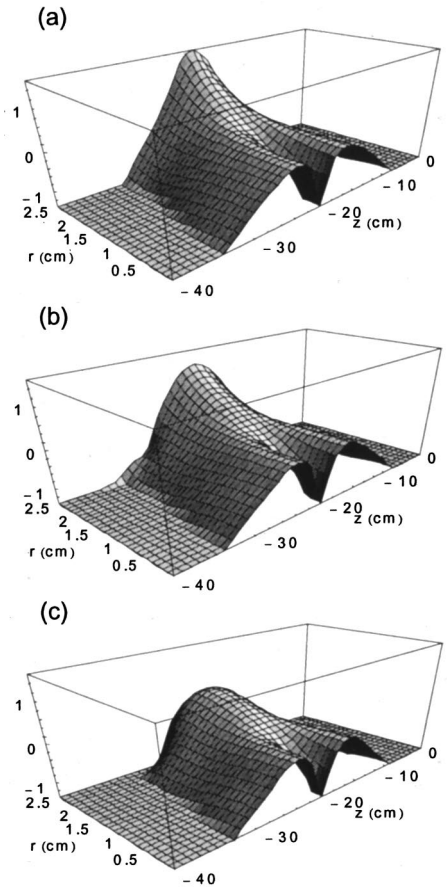

FIG. 8. Profiles of the absorbed power, in log scale, computed with the H-TG model for a magnetized plasma, at $p_{\mathrm{Ar}}=51$ mTorr, $B_0=100$ G, $n_0=2\times10^{12}\,\mathrm{cm}^{-3}$, and parallel antenna currents. (a) Uniform plasma, (b) $n_{\mathrm{edge}}=0.5n_0$, and (c) $n_{\mathrm{edge}}=0$.

propagating helicons. Another reason for the suppression of short wave absorption is the appearance of a low density region adjoining the plasma boundary, which is nontransparent for the short helicons and plays the same role as the vacuum gap between the antenna and plasma column.[17,19] The TE-H spectral peak decreases with n_{edge}, apparently due to reduction of the cavity resonances.

IV. ABSORPTION PROFILES

Spatial profiles of the specific absorbed power, $p_a(r,z)$, were computed using Eq. (11). Figure 7(a)[42] shows in log scale, $\log_{10}(p_a)$, the profile for a uniform unmagnetized plasma at the same conditions as in Fig. 2. (Note p_a has dimensions of mW/cm^3, and the current in each of antenna loops is equal to 1 A throughout this section.) In this case, the skin depth $\delta_c\approx0.5r_0$, but the penetration depth is found to be somewhat less than δ_c. It is equal to some average over the spectrum shown in Fig. 2(b). As long as E_θ is the only electric field component excited at $B_0=0$, the absorption vanishes on the axis for $m=0$ excitation. The axial width of the absorption profile is mainly defined by the total width of the double antenna. At densities lower than in Fig. 7(a), the shape of the absorption profile does not change substantially, but its magnitude drops approximately as n_0. At higher densities, the profile substantially shrinks in the radial direction whereas its magnitude increases only slightly, as seen from Fig. 7(b). The influence of the plasma nonuniformity on the absorption profile is seen from Fig. 7(c). The absorption peak decreases, but the profile spreads radially from the plasma edge. As a result, the total absorption is found to remain practically constant. This is so at high central densities, when the mean skin depth is less than $\approx r_0/2$. At lower densities, the absorption area is extended radially up to the plasma center and thus cannot vary considerably with density, so that the total absorption drops with decreasing edge density.

The absorption profile substantially differs when the plasma is magnetized, $\omega_{ce}>\omega|\gamma_e|$. Figure 8(a) shows, on a log scale, the profile computed with H-TG model at the same conditions as in Fig. 7, but with $B_0=100$ G. The helicon radiation results in that the profile is considerably extended axially, especially in the bulk plasma, as compared with that at zero magnetic field. An absorption peak under the antenna is practically the same in amplitude as in the $B_0=0$ case, but is sharper. The peak is formed mainly by the power deposition from the TG waves and, to a minor degree, from evanescent helicons, since the TG amplitudes are much higher. As long as the penetration depths of the TG waves are less than the skin depth, the near-antenna peak is sharper in the

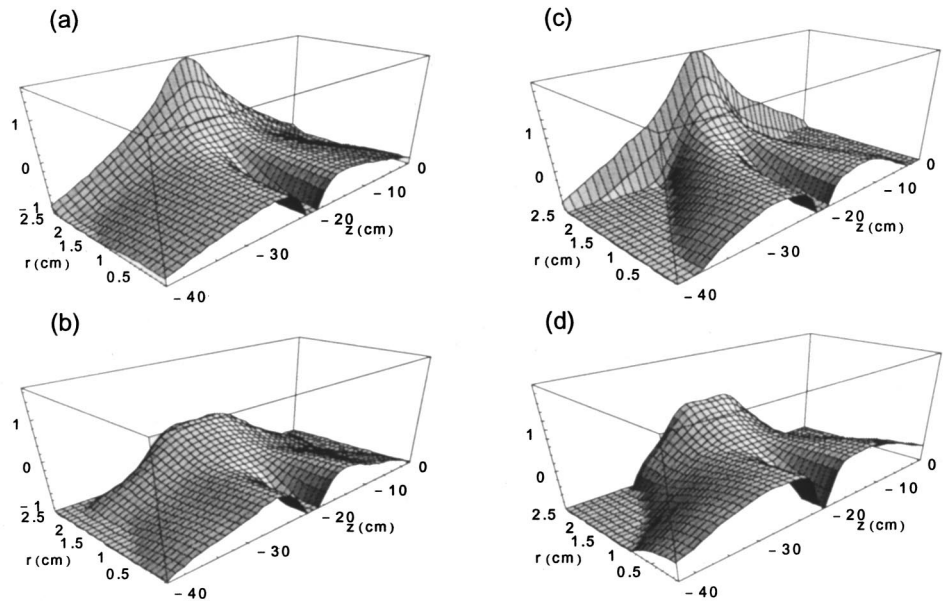

FIG. 9. Profiles of the absorbed power, in log scale, computed with the H-TG model for (top) uniform and (bottom) nonuniform plasma with $n_{edge}=0$, at $p_{Ar}=51$ mTorr, $B_0=300$ G, and parallel antenna currents. (a) and (b): $n_0=2\times10^{12}$ cm^{-3}; (c) and (d): $n_0=2\times10^{13}$ cm^{-3}.

radial direction than that at $B_0=0$. In contrast with unmagnetized case, one can see in Fig. 8(a) a finite on-axis absorption due to appearance of the E_z electric field in magnetized plasma. For the parallel excitation, $E_z=0$ in the antenna midplane, $z=-20$ cm, as there are no waves reflected from the ends, and thus the absorption is zero at this position on axis.

Figures 8(b) and 8(c) show the absorption profiles computed for the nonuniform plasma with the same central density as in Fig. 8(a). One can see that the shape of the profile near the plasma center depends only slightly on the nonuniformity, whereas the near-antenna peak decreases. As seen from Fig. 8(c), the peak holds even at zero edge density, but its position shifts somewhat from the plasma surface. In this case, the surface conversion of the helicon waves into TG waves does not occur. Instead, the bulk conversion is stimulated at the density gradient.[16] The absorption is proportional to the density growing inward from the edge, whereas the generation of the TG waves intensifies with increase of the density gradient toward the plasma edge. The position of the absorption peak is defined by a competition of these two factors.

Increasing magnetic field results in the decrease of the helicon damping [see Eq. (22) and Fig. 5(c)]. For this reason, the absorption profile in the bulk plasma extends far from antenna due to enhanced radiation of helicon waves, as seen from Fig. 9(a) computed at the same conditions as Fig. 8(a), but at $B_0=300$ G. The near-edge absorption far from antenna is found to be higher because the TG amplitudes increase with magnetic field, as clear from Eq. (24). The under-antenna absorption peak is approximately the same in amplitude as in previous cases, but falls faster radially due to stronger damping of the TG waves [see Eq. (21) and Fig. 5(c)]. Decrease of the edge density changes the absorption in the bulk plasma only slightly but substantially reduces the under-antenna peak and shifts it inward at very low edge density, as seen from Fig. 9(b). At higher center density, the absorption profile is narrower in the axial direction, as shown in Fig. 9(c). The reason for this can be understood from a general property of the wave packages: the width of a localized wave profile in configuration space is inversely proportional to its width in k-space. As long as the width of the helicon k-spectrum, $\approx k_{up}$, increases with density, the width of the helicon wave profile in the configuration space becomes narrower with density. One can see from Fig. 9 that the near-edge absorption due to the mode conversion is more pronounced at higher density, as a result of stronger damping of the TG waves. As seen from Fig. 9(d), the under-antenna peak decreases with edge density, but not so strongly as it does at lower center density. At the same time, the bulk absorption increases and extends axially due to enhanced radiation of helicons.

Figure 10 shows the absorption profiles computed with neglect of the TG waves (TE-H model) at the same conditions as in Fig. 9. One can see that the spatial distribution of the absorption alters dramatically: the profile becomes much more uniform, and is 1–2 orders of magnitude lower. The under-antenna absorption is very weak at lower densities [see Fig. 10(a)]. At higher density, a peak formed by evanescent helicons exists in uniform plasma but practically disappears in nonuniform plasma [compare Figs. 10(b) and 10(c)].

Figure 11, as compared with Fig. 8, demonstrates the influence of pressure (collision frequency) on the absorption profile. One can see from Fig. 11(a) that at lower pressure of 6 mTorr the absorption is concentrated in a thin edge layer because damping rates of the TG waves are higher than they are at 51 mTorr. Irradiated by the antenna, helicon waves propagate along the plasma column and preferentially transfer the energy to the TG waves near the edge rather than suffer from the collisional damping in the bulk plasma. One can see from Fig. 11(b) that in a nonuniform plasma the center absorption is enhanced whereas the absorption due to the mode conversion shifts inward from the edge. The profile computed with TE-H model [see Fig. 11(c)] demonstrates the appearance of reflected waves and formation of standing pattern. This profile is asymmetric around the antenna midplane

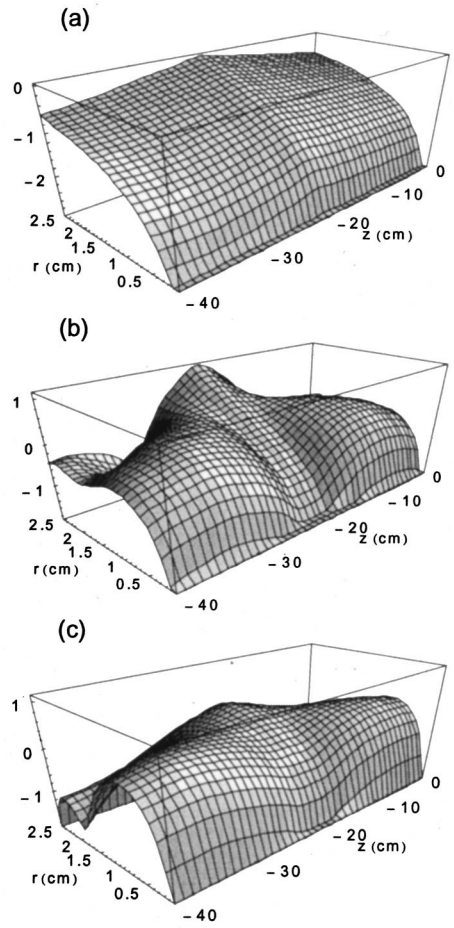

FIG. 10. Absorption profiles, in log scale, computed with the TE-H model, at $p_{\mathrm{Ar}}=51$ mTorr, $B_0=300$ G, and parallel antenna currents. (a) Uniform plasma with $n_0=2\times10^{12}\,\mathrm{cm}^{-3}$; (b) uniform and (c) nonuniform ($n_{\mathrm{edge}}=0$) plasma with $n_0=2\times10^{13}\,\mathrm{cm}^{-3}$.

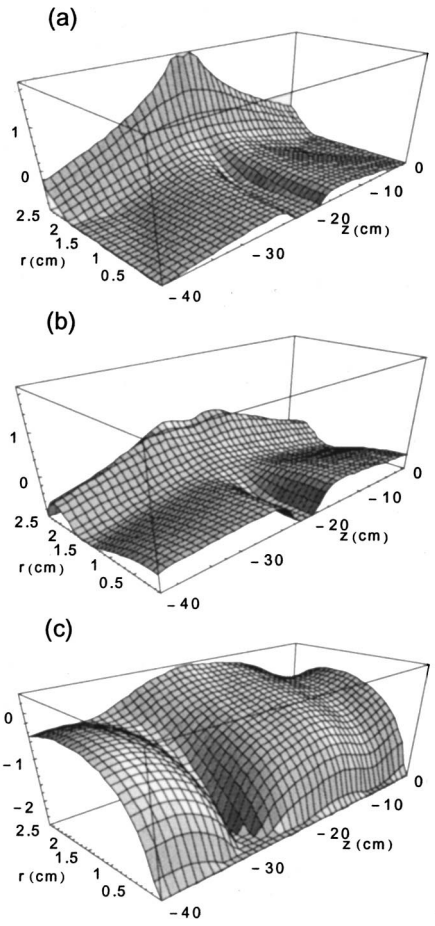

FIG. 11. Absorption profiles, in log scale, at $p_{\mathrm{Ar}}=6$ mTorr, $B_0=100$ G, $n_0=2\times10^{12}\,\mathrm{cm}^{-3}$, and parallel antenna currents. H-TG model for (a) uniform and (b) nonuniform plasma with $n_{\mathrm{edge}}=0$; (c) TE-H model for the uniform plasma.

as a result of the asymmetric antenna position relative to the reflecting ends.

Absorption profiles for the anti-parallel currents in antenna loops are presented in Fig. 12. In this case, the long modes are excluded from the antenna spectrum and thus from the absorption spectrum [see Figs. 1 and 4(c)]. For this reason, the near-antenna peak in Fig. 12(a) is very steep radially, as it is formed by the short, strongly damping TG waves. As long as the reduction of the edge density just cuts the contribution of short modes, the absorption substantially decreases in nonuniform plasma, as seen from Fig. 12(b). The profile computed with the TE-H model is much more extended from the antenna, as shown in Fig. 12(c).

To quantitatively characterize the spatial partition of absorption, we computed the fractions of the rf power absorbed in various parts of the plasma column. The portion of total power deposited in the axial part of the plasma column, centered at the antenna midplane and 4 cm long, was defined as the under-antenna absorption, P_{ua}. The portion absorbed in near-boundary radial layer of 2 mm width, which comprises 15% of the total plasma volume, was considered as the edge absorption, P_{ed}. We also computed the portion P_{ue} absorbed in a 2 mm edge layer of the under-antenna region, of fractional volume about $\eta_{ue}\approx0.4\%$.

Figure 13 shows the variation with density of all three fractions computed for the uniform plasma, 51 mTorr, and parallel excitation. They are found to be weakly sensitive to the density variation. As seen from Fig. 13(a), increasing magnetic field gives rise to a decrease of the P_{ua}/P_a ratio, as a result of increasing helicon wave radiation. On the contrary, P_{ed}/P_a increases with magnetic field due to decrease of the TG damping lengths. A competition of these two tendencies results in that P_{ue}/P_a depends only slightly on the magnetic field, as seen from Fig. 13(c). This fraction can be two orders of magnitude higher than the fractional volume, η_{ue}. All power fractions computed with the TE-H model are found to be much lower, as shown in Fig. 13 by dashed curves. The power fractions computed for the anti-parallel excitation at 51 mTorr and for the parallel excitation at 6 mTorr demonstrate, in general, similar tendencies. However, specific results reflect changes in the helicon wave emissivity, as discussed above. For instance, all dependencies are more pronounced at 6 mTorr; the under-antenna absorption is insensitive to the magnetic field for the anti-parallel excitation. Note that the power absorption at high pressures does not demonstrate, neither in experiment nor in calculations, any considerable peculiarities in the range of lower hybrid resonance ($B_0\approx678$ G), as it does at low pressures.[38]

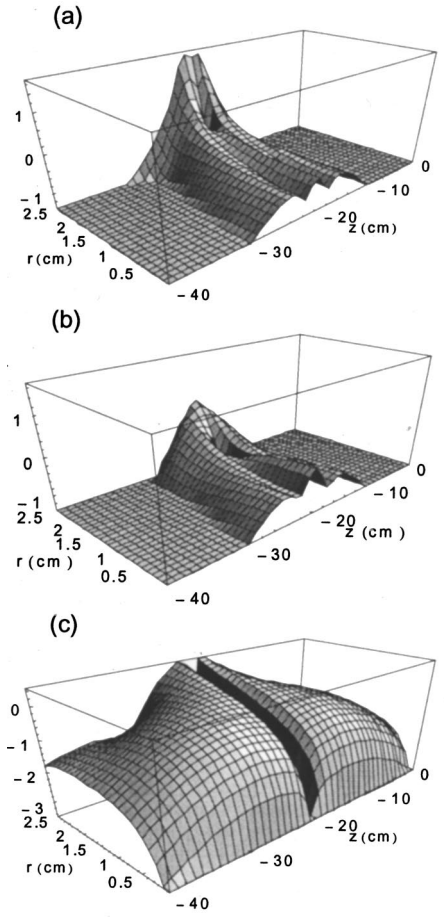

FIG. 12. The same as in Fig. 11, but at $p_{\mathrm{Ar}}=51$ mTorr, $B_0=100$ G, $n_0=1\times10^{13}\,\mathrm{cm}^{-3}$, and anti-parallel antenna currents.

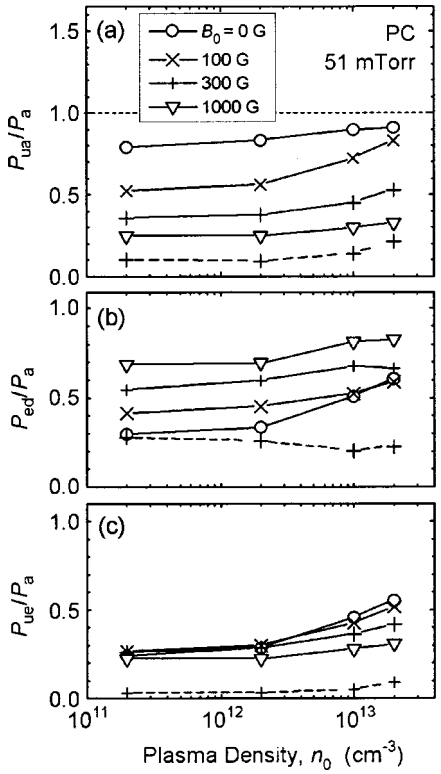

FIG. 13. Fractions of the total power absorbed in the under-antenna region (a), edge layer (b), and edge layer of the under-antenna region (c). Solid and broken curves were computed, respectively, with the H-TG model at various B_0, and with the TE-H model at 300 G. $p_{\mathrm{Ar}}=51$ mTorr and parallel currents in the antenna loops.

The influence of the plasma nonuniformity on the under-antenna absorption can be seen from Fig. 14 computed with the H-TG model. The variation of P_{ua}/P_a with the edge density is very weak at zero magnetic field, but is stronger at 300 G. The edge under-antenna absorption clearly demonstrates more substantial dependence on the edge density. P_{ue}/P_a is found to scale roughly as $n_{\mathrm{edge}}^{1/2}$ in unmagnetized plasma, and almost linearly with n_{edge} at 300 G. At 6 mTorr, the under-antenna absorption turns out to depend much stronger on the edge density.

V. PLASMA LOAD RESISTANCE

The dependence of plasma resistance on density was computed for various conditions with the use of Eq. (12). Figure 15(a) shows the load resistance of unmagnetized, uniform plasma column excited with parallel currents, at two values of Ar pressure. Also shown is the variation of the collisional skin depths with density [see Eq. (15)]. The resistance first increases nearly linearly, reaches the maximum value at some density, and then slightly drops. The maximum occurs when the skin depth drops down to the value of order of $0.4r_0$. At this level, the azimuthal countercurrent generated in plasma becomes strong enough to cancel the antenna field in the bulk plasma. Beyond the maximum, the resistance slightly decreases due to a cooperative effect of several

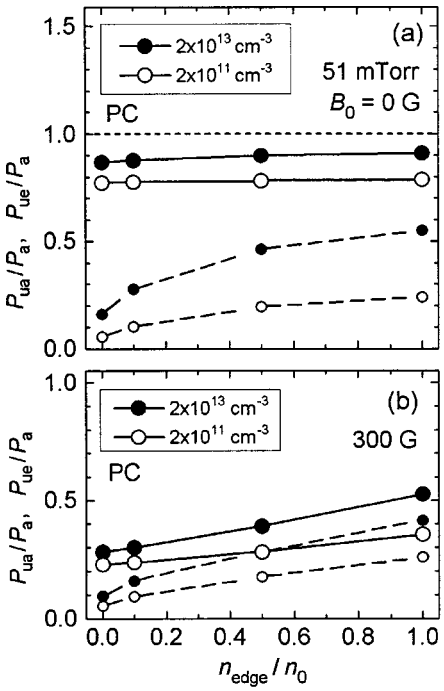

FIG. 14. Fractions of the total power absorbed in the under-antenna region (solid curves) and in its edge layer (dashed curves) of the nonuniform plasma column, at various edge densities and $n_0=2\times10^{13}\,\mathrm{cm}^{-3}$ (solid symbols) and $n_0=2\times10^{11}\,\mathrm{cm}^{-3}$ (open symbols). $p_{\mathrm{Ar}}=51$ mTorr and parallel antenna currents. (a) $B_0=0$ G and (b) $B_0=300$ G.

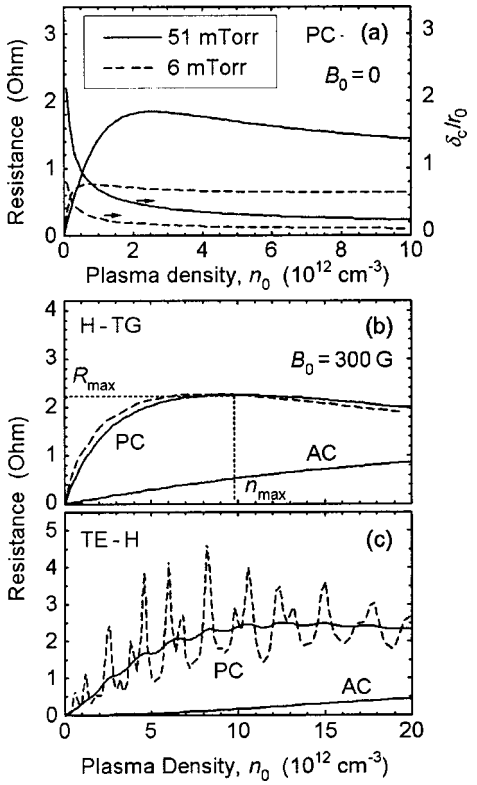

FIG. 15. Dependencies of the plasma resistance on density for the uniform plasma and Ar pressures of 51 mTorr (solid curves) and 6 mTorr (dashed curves). Unmagnetized plasma (a); $B_0 = 300$ G and H-TG approximation (b) and TE-H approximation (c). PC and AC refer to the parallel and anti-parallel antenna currents. At 51 mTorr, the resistance acquires the maximum value, R_{max}, at a characteristic density n_{max}.

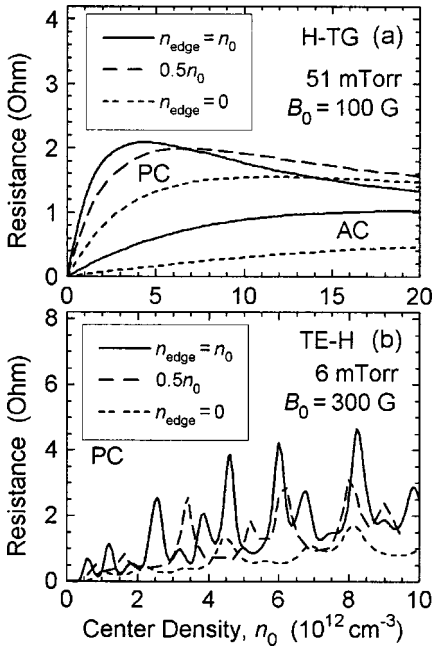

FIG. 16. Dependencies of the plasma resistance on the center density, at various edge densities. (a) $p_{Ar} = 51$ mTorr, $B_0 = 100$ G, and H-TG approximation, and (b) $p_{Ar} = 6$ mTorr, $B_0 = 300$ G, and TE-H approximation.

factors, including shrinking of the absorption area, decrease of the field amplitudes due to shielding effect of the plasma current, increase of collision frequency through the Coulomb addend, and the depletion of the antenna spectrum. One can see from Fig. 15(a) that in the density range above $1 \times 10^{12}\,\mathrm{cm}^{-3}$ the resistance at 51 mTorr is more than twice as large as that at 6 mTorr. An apparent reason is that the skin depth and thus the spatial area of the rf power deposition are reduced at lower pressure.

The resistance of a uniform plasma column computed with the H-TG model at $B_0 = 300$ G is shown in Fig. 15(b). For parallel antenna currents, the initial growth rate of the resistance is slower than at zero magnetic field. The maximum value of resistance at 51 mTorr, R_{max}, is only a little higher whereas the position of maximum, n_{max}, is considerably higher than those values at $B_0 = 0$. At 6 mTorr, both the maximum resistance and corresponding density are considerably higher than at zero magnetic field. The higher level of density needed to saturate the resistance in magnetized plasma is a result of substantial redistribution of plasma currents. As concluded in Sec. IV by comparing Figs. 7 and 9, the under-antenna region, where the fields are the most intense, is radially greatly reduced while axially only slightly extended in the presence of the magnetic field. The reason was seen in that the near-surface plasma current is mainly due to TG waves penetrating a distance much smaller than the skin depth. So, the total area occupied by the intense plasma countercurrent drops with increasing B_0, and thus higher density is needed to induce the current strong enough for canceling the fields in the bulk plasma. As seen from Fig. 15(b), the variation of resistance with density is similar at both pressures. The reason is that the helicon waves directly excited by the antenna are dominantly absorbed through the mode conversion into TG waves. This cooperative mechanism is weakly sensitive to the collisions. The resistance turns out to be much lower for anti-parallel antenna currents [see Fig. 15(b)] because the antenna spectrum in this case does not include long modes and thus excitation of low damping helicons is suppressed.

The resistance computed with the TE-H model is shown in Fig. 15(c) for the same conditions as in Fig. 15(b). At 51 mTorr, the initial growth rate is lower than that predicted by the H-TG model, but the level of saturation is nearly the same. The resistance curve is slightly rippled due to the cavity resonances, which are well suppressed at such a high pressure. These resonances become pronounced with decreasing damping of helicon waves. As seen from Fig. 15(c), the resistance peaks are very sharp at lower pressure of 6 mTorr, and especially in the range of smaller densities where collisions are reduced. Each peak is split into two, corresponding to the first and second radial resonances. Another way to reduce the helicon damping is to raise the magnetic field, as seen from Eq. (22). Even at 51 mTorr, the resistance curves computed with the TE-H model turn out to display distinct resonances at magnetic fields above 500 G (not shown). As seen from comparison of Figs. 15(b) and 15(c), the TE-H resistance for anti-parallel currents is very low.

Figure 16(a) shows the influence of radial plasma nonuniformity on the plasma resistance computed with the H-TG model for the parabolic profile, Eq. (1). One can see

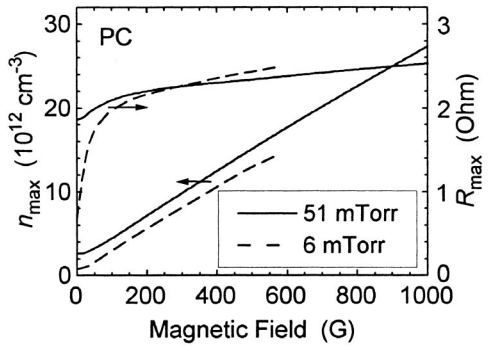

FIG. 17. Dependencies on the magnetic field of the plasma resistance maximum, R_{max}, and characteristic density, n_{max}, for the uniform plasma and Ar pressures of 51 mTorr (solid curves) and 6 mTorr (dashed curves).

that initial growth rate of the resistance curve is less in nonuniform plasma. For parallel currents, the saturation occurs at higher n_0. This behavior may be understood by considering the influence of nonuniformity upon the plasma currents. Indeed, the resistance saturation occurs when the plasma countercurrent becomes strong enough to cancel the antenna fields in the bulk plasma. As long as the countercurrent flows mainly on the edge, the saturation in nonuniform plasma occurs when the value of n_{edge} (if it is not too low) is approximately equal to the value of density at which the effect arises in the uniform case. One can see from Fig. 16(a) that the resistance of a nonuniform plasma column may be higher at high n_0, even with zero n_{edge}. Although the nonuniformity cuts out the high components of the spectrum, the total absorption can be raised through the increasing contribution of the long modes. With parallel currents, the dependence of resistance on nonuniformity is similar at any magnetic field including $B_0=0$. One can see from Fig. 16(a) that for anti-parallel currents the decrease of edge density strongly reduces the resistance, and the maximum does not occur in the range of reasonable densities. This is found to be the case at any magnetic field. Resistance curves computed with the TE-H model for the nonuniform plasma are shown in Fig. 16(b). They are multi-peaked due to excitation of the cavity resonances. At lower n_{edge}, the mean level of the resistance decreases; the peaks are reduced and change positions, but survive even at zero edge density.

Theoretical scaling of the resistance with magnetic field; that is, dependencies on B_0 of the maximum resistance, R_{max}, and of its position, n_{max}, is shown in Fig. 17. It is computed with the H-TG model for a uniform plasma. As seen, the maximum values of resistance for both 51 and 6 mTorr are very close and vary only slightly above 100 G. Below 100 G, the effect of magnetic field is more pronounced at the lower pressure of 6 mTorr. Positions of the resistance maxima are also close above 100 G for both pressures and depend linearly on the magnetic field. For a nonuniform plasma, one can find a similar resistance scaling, but the resistance maxima become somewhat lower and occur at higher center densities.

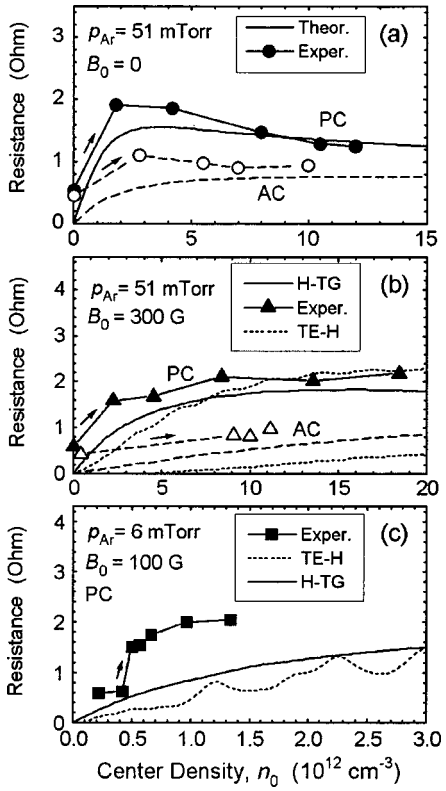

FIG. 18. Measured antenna load resistance and computed with the H-TG model plasma resistance vs center density, for the parallel (solid symbols and solid curves) and anti-parallel (open symbols and dashed curves) antenna currents. Arrows show experimentally measured density jumps. Dotted curves in (b) and (c) are computed with the TE-H model. (a) $p_{Ar}=51$ mTorr and $B_0=0$ G; (b) $p_{Ar}=51$ mTorr and $B_0=300$ G; and (c) $p_{Ar}=6$ mTorr and $B_0=100$ G. In (a) and (b), theoretical curves were computed with $n_{edge}=0.5n_0$, for the parallel currents, and with $n_{edge}=n_0$, for the anti-parallel currents. In (c), $n_{edge}=0.2n_0$.

VI. COMPARISON OF EXPERIMENT AND THEORY

In Fig. 18, measured values of the antenna load resistance are compared with theoretical dependencies of the plasma resistance computed with both the H-TG and TE-H models. Computations were performed with density profiles like those measured in experiment. Experimental resistance includes, in contrast with theoretical one, an additional part associated with nonplasma losses in the rf circuitry and metal environment, which amount to a few tenths of Ohm but are not known exactly. To within this addend and considering the alteration of the plasma profile with varying density, one can see in Fig. 18(a) that theory gives a good fit to the experimental data at zero magnetic field (ICP discharge), for both the parallel and anti-parallel antenna currents. One can see in Fig. 18(b) that the agreement of the H-TG theory with experiment is good over the whole range of densities for 51 mTorr and 300 G, with both relative directions of the antenna currents. With parallel currents, the agreement is poorer but still satisfactory with TE-H theory: it underestimates the resistance at lower densities while overestimates it at higher densities. However, the agreement is much worse for the case of anti-parallel currents, as the TE-H approach yields too low values of resistance.

Figure 18(c) compares the resistances at the lower pres-

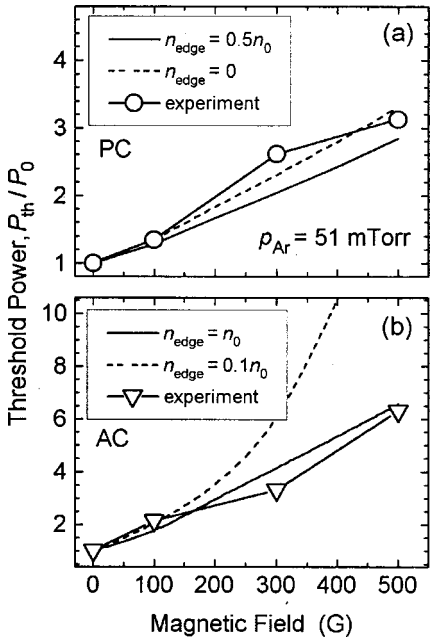

FIG. 19. Measured and computed with the H-TG model dependencies on the magnetic field of the threshold power for the density jump for (a) parallel and (b) anti-parallel antenna currents, at $p_{Ar}=51$ mTorr. Threshold power is normalized to that for the jump at $B_0=0$ G.

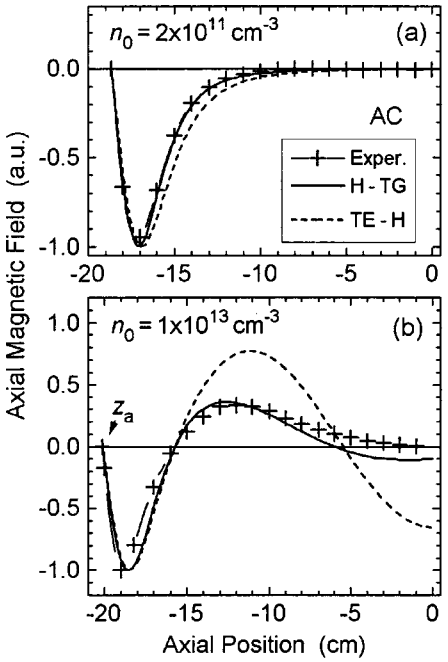

FIG. 20. Axial profiles of the B_z magnetic field on the axis, as measured (crosses) and computed with the H-TG (solid curves) and TE-H (dashed curves) models, for the anti-parallel antenna currents, $p_{Ar}=51$ mTorr, and $B_0=300$ G. (a) Low density mode before the jump, $n_0=2\times10^{11}$ cm^{-3}, and (b) high density mode after the jump, $n_0=1\times10^{13}$ cm^{-3}.

sure of 6 mTorr. In this case, computations were performed with $n_{edge}=0.2n_0$ because the measured density profile is more peaked than in the case of 51 mTorr. The H-TG theory predicts a resistance about 1.5 times less than in the measurements, and does not predict so strong density jump as it is in experiment. The disagreement is thought to result from the kinetic effects neglected in the model, and from substantial change in density profile before and after the jump. The prediction of the TE-H approach is worse as it yields a resistance 2–4 times lower than the experimental one. Note that in Fig. 18(c) there are neither experimental points at high densities for parallel currents nor any points at all for anti-parallel antenna currents. The reason is that ignition of the discharge was not possible at 6 mTorr with anti-parallel excitation, in spite of the fact that computations predict a considerable absorption. The reason for this is not known for sure but is thought to be a problem of discharge initiation rather than of power absorption. With parallel antenna currents, the discharge could be initiated at 6 mTorr. However, except for very high fields above 500 G, it produced much poorer plasma density and met problems with coupling to the high density mode, in contrast with the discharge at 51 mTorr and the same input power.

Computed dependencies of the plasma resistance on density can be used to predict the jumps into the high density mode by considering the power balance in the discharge,[16,19] which is known to be of primary importance as compared with the particle balance.[39,40] Such a semi-qualitative approach permits one, in particular, to estimate the threshold in input power that is needed to initiate the density jump. Figure 19 shows computed and measured dependencies on the magnetic field of the threshold power, P_{th}, normalized to that needed for the jump at zero magnetic field, P_0. One can see from Fig. 19(a) that, for the case of parallel antenna currents, experimental scaling of P_{th} with magnetic field is nearly linear and fits well with the theoretical scaling, the latter being insensitive to plasma nonuniformity. For anti-parallel currents, the scaling is also nearly linear [see Fig. 19(b)], but it fits well only to the theoretical curve computed for a nearly uniform plasma profile.

The axial profiles of the ac magnetic field, $B_z(r=0)$, are compared in Fig. 20 for the case of anti-parallel excitation. Figure 20(a) shows the normalized profiles in the low density mode, before the density jump. As seen, both H-TG and TE-H models yield close profiles well fitted to the experimental one. For the high density mode [see Fig. 20(b)] theoretical curves were adjusted for phase to fit the nodes of B_z. The H-TG approach is found to give much better fit to the experimental data. The TE-H model strongly overestimates the radiation of helicons into remote plasma. It is apparently a general shortcoming that is inherent in the TE-H model, as is clear from the absorption profiles considered in Sec. IV.

VII. SUMMARY AND CONCLUSIONS

A comparative examination of the antenna spectrum, wave dispersion, and power absorption spectra as functions of the axial wave number allows one to estimate the relative role of various factors in rf power absorption and thus to determine the scaling laws. The antenna spectrum defines the regions of k-space where waves can, in principle, be efficiently excited. Whether or not they would be excited is governed by the helicon dispersion. The simplest dispersion curves for an unbounded, uniform plasma give a clear pic-

ture of this. Excited helicons are absorbed mainly via mode conversion into TG waves at the plasma boundary and in regions of strong density gradient.

The absorption k-spectrum includes three different regions. The principal absorption is provided by the modes with intermediate wavelengths in the region of helicon transparency, Eq. (19). Inside this region, the most efficient absorption comes from helicon modes whose E_θ fields are maximum near the plasma boundary, Eq. (25). A considerable absorption may be associated with long modes from the region of the decreased skin effect, $k<k_{\mathrm{low}}$. Short evanescent modes, $k>k_{\mathrm{up}}$, contribute weakly to absorption. In a nonuniform plasma, the short-wave part of the absorption spectrum gradually weakens with decreasing edge density.

The double loop $m=0$ antenna with parallel currents efficiently generates the long waves with lengths exceeding twice the distance between the loops. For this reason, the absorption can suffer from the depletion of antenna spectrum at high densities and/or low magnetic fields, when the upper excitation boundary, k_{up}, gets to the region of the poor spectral intensity of the antenna. On the contrary, the antenna with anti-parallel currents generates the short modes and gives rise to substantial absorption at high densities and/or decreased magnetic fields, when its spectral intensity is high for the wave numbers above k_{low}.

The most efficient absorption occurs in the under-antenna region due to TG waves and, in a minor degree, due to evanescent helicon modes. The TG waves give rise to a sharp absorption peak, which increases with TG wave damping and is located in the near-boundary layer just underneath the antenna. This is consistent with the results of experiments[41] where the optical emission from the ''hot spots'' located at the periphery of the under-antenna region was measured to increase with pressure. The absorption in remote plasma is stimulated by the helicon wave radiation; it is enhanced at lower densities and especially at higher magnetic fields and lower pressures. The radiated waves suffer from mode conversion, which considerably reduces the axial penetration depth, as compared with the collisional depth, and gives rise to the enhanced near-edge absorption. The plasma nonuniformity increases the helicon radiation and reduces the near-antenna absorption. At very low edge densities, the bulk mode conversion prevails over the surface conversion, and the absorption peak moves from the boundary into the bulk plasma.

With increasing density, the plasma load resistance grows up and then saturates when the countercurrent induced in plasma becomes strong enough to cancel in the plasma interior the magnetic flux produced by the antenna current. At zero magnetic field, the resistance magnitude decreases with the collision frequency, but it is practically independent of the collisions in magnetized plasma. The characteristic density at which saturation of resistance occurs increases nearly linearly with magnetic field, as a result of the alteration of the area occupied by the plasma current. At zero field, this area is defined by the skin size. In magnetized plasma, the countercurrent is generated mainly by the TG waves near the plasma edge. At high pressures, the damping length of the TG wave is shorter than the skin depth and scales as B_0^{-1}, so that the current area shrinks radially with the same dependence. In nonuniform plasma, the resistance increases with density at a lower rate because the intensity of mode conversion, and thus the near-surface countercurrent, are reduced. The resistance maximum is reached at higher density but is practically the same in magnitude as in uniform plasma.

A detailed comparison of numerous experimental data with theoretical computations on the basis of theory considering TG waves shows a good agreement of the results, including the plasma load resistance, thresholds for density jumps, and field profiles, over a broad range of parameters (see also Ref. 19). Therefore, this theoretical approach seems to be satisfactory for the characterization of power absorption in high pressure helicon plasmas. The approach neglecting the excitation of the TG waves yields reasonable values of the plasma resistance at strong helicon damping, but is unsatisfactory at low densities, and especially at low pressures and high magnetic fields when helicon damping is so weak as to give rise to the cavity resonances. With neglect of the TG waves, the fields were found to penetrate much deeper into remote plasma, in disagreement with measurements, and thus to result in absorption that is too extended from the antenna.

ACKNOWLEDGMENTS

The authors appreciate continuous encouragement of Professor Y. Kawai.

K.P.S. gratefully acknowledges support of his visit to Kyushu University by Venture Business Laboratory.

[1] R. W. Boswell and F. F. Chen, IEEE Trans. Plasma Sci. **25**, 1229 (1997).
[2] F. F. Chen and R. W. Boswell, IEEE Trans. Plasma Sci. **25**, 1245 (1997).
[3] A. J. Perry, D. Vender, and R. W. Boswell, J. Vac. Sci. Technol. B **9**, 310 (1991).
[4] N. Jiwari, H. Iwasawa, A. Narai, H. Sakaue, H. Shindo, T. Shoji, and Y. Horiike, Jpn. J. Appl. Phys. **32**, 3019 (1993).
[5] G. R. Tynan, A. D. Bailey III, G. A. Campbell, R. Charatan, A. de Chambrier, G. Gibson, D. J. Hemker, K. Jones, A. Kuthi, C. Lee, T. Shoji, and M. Wilcoxson, J. Vac. Sci. Technol. A **15**, 2885 (1997).
[6] F. R. Chang Díaz, Trans. Fusion Technol. **35**, 87 (1999).
[7] R. W. Boswell, Plasma Phys. Controlled Fusion **26**, 1147 (1984).
[8] F. F. Chen, Plasma Phys. Controlled Fusion **33**, 339 (1991).
[9] G. G. Borg and I. V. Kamenski, Phys. Plasmas **4**, 529 (1997).
[10] A. W. Degeling, C. O. Jung, R. W. Boswell, and A. R. Ellingboe, Phys. Plasmas **3**, 2788 (1996).
[11] F. F. Chen and D. D. Blackwell, Phys. Rev. Lett. **82**, 2677 (1999).
[12] K. P. Shamrai and V. B. Taranov, Plasma Sources Sci. Technol. **5**, 474 (1996).
[13] G. G. Borg and R. W. Boswell, Phys. Plasmas **5**, 564 (1998).
[14] I. V. Kamenski and G. G. Borg, Comput. Phys. Commun. **113**, 10 (1998).
[15] Th. Enk and M. Krämer, Phys. Plasmas **7**, 4308 (2000).
[16] K. P. Shamrai, Plasma Sources Sci. Technol. **7**, 499 (1998).
[17] D. Arnush and F. F. Chen, Phys. Plasmas **5**, 1239 (1998).
[18] S. Cho and J.-G. Kwak, Phys. Plasmas **4**, 4167 (1997).
[19] S. Shinohara and K. P. Shamrai, Plasma Phys. Controlled Fusion **42**, 865 (2000).
[20] A. Fukuyama and Y. Ichida, in *Proceedings of the International Conference on Plasma Physics*, Nagoya, 1996, edited by H. Sugai and T. Hayashi (Japan Society of Plasma Science and Nuclear Fusion Research, Nagoya, 1997), Vol. 2, p. 1342.
[21] Y. Mouzouris and J. E. Scharer, Phys. Plasmas **5**, 4253 (1998).
[22] I. V. Kamenski and G. G. Borg, Phys. Plasmas **3**, 4396 (1996).
[23] D. A. Schneider, G. G. Borg, and I. V. Kamenski, Phys. Plasmas **6**, 703 (1999).

[24]D. Arnush, Phys. Plasmas **7**, 3042 (2000).
[25]F. F. Chen, D. Arnush, J. D. Evans, and D. D. Blackwell, in *Proceedings of the International Congress on Plasma Physics & 25th EPS Conference on Controlled Fusion and Plasma Physics*, Prague, 1998, edited by P. Pavlo (European Physical Society, Prague, 1998), Europhysics Conference Abstracts, Vol. 22C, p. 2655.
[26]T. Lho, N. Hershkowitz, J. Miller, W. Steer, and G. H. Kim, Phys. Plasmas **5**, 3135 (1998).
[27]K. P. Shamrai, V. F. Virko, H.-O. Blom, V. P. Pavlenko, V. B. Taranov, L. B. Jonsson, C. Hedlund, and S. Berg, J. Vac. Sci. Technol. A **15**, 2864 (1997).
[28]X. M. Guo, J. Scharer, Y. Mouzouris, and L. Louis, Phys. Plasmas **6**, 3400 (1999).
[29]N. Hershkowitz, IEEE Trans. Plasma Sci. **26**, 1610 (1998).
[30]S. Shinohara and K. Yonekura, Plasma Phys. Controlled Fusion **42**, 41 (2000).
[31]K. P. Shamrai, V. P. Pavlenko, and V. B. Taranov, Plasma Phys. Controlled Fusion **39**, 505 (1997).
[32]K. P. Shamrai and V. B. Taranov, Plasma Phys. Controlled Fusion **36**, 1719 (1994).
[33]B. Fisher, M. Krämer, and Th. Enk, Plasma Phys. Controlled Fusion **36**, 2003 (1994).
[34]F. F. Chen, Phys. Fluids **22**, 2346 (1979).
[35]S. Shinohara, N. Kaneda, and Y. Kawai, Thin Solid Films **316**, 139 (1998).
[36]T. H. Stix, *Theory of Plasma Waves* (McGraw-Hill, New York, 1962).
[37]S. Shinohara and Y. Kawai, Jpn. J. Appl. Phys., Part 2 **35**, L725 (1996).
[38]Y. Sakawa, T. Takino, and T. Shoji, Phys. Plasmas **6**, 4759 (1999).
[39]M. A. Lieberman and A. J. Lichtenberg, *Principles of Plasma Discharges and Materials Processing* (Wiley, New York, 1994).
[40]M. A. Lieberman and R. W. Boswell, J. Physique **8**, Pr7-145 (1998).
[41]K. Nakamura, K. Suzuki, and H. Sugai, Jpn. J. Appl. Phys. **34**, 2152 (1995).
[42]See EPAPS Document No. E-PHPAEN-8-057109 for color figures. This document may be retrieved via the EPAPS homepage (http://www.aip.org/pubservs/epaps.html) or from ftp.aip.org in the directory /epaps/. See the EPAPS homepage for more information.